Materials Science & Engineering C 117 (2020) 111336

Contents lists available at ScienceDirect

Materials Science & Engineering C

journal homepage: www.elsevier.com/locate/msec

Optimizing ibuprofen concentration for rapid pharmacokinetics on biocompatible zinc-based MOF-74 and UTSA-74

Shane Lawson, Kyle Newport, Kurt Schueddig, Ali A. Rownaghi, Fateme Rezaei*

Department of Chemical & Biochemical Engineering, Missouri University of Science and Technology, Rolla, MO 65409-1230, United States

ARTICLE INFO

Keywords:
Biocompatible MOFs
Ibuprofen
Drug delivery

ABSTRACT

Metal-organic frameworks (MOFs) have potential as drug carriers on the basis of their surface areas and pore volumes that allow for high loading and fast release. This study investigated two biocompatible MOFs – Zn MOF-74 and UTSA-74 – for ibuprofen delivery. The effect of drug loading was studied by impregnating the MOFs with 30, 50, and 80 wt% ibuprofen. The samples were characterized by scanning electron microscopy (SEM), X-ray diffraction (XRD), and N_2 physisorption. From SEM, the MOF structures were maintained at 30 wt% ibuprofen, however, became agglomerated at 50–80 wt% loading, as the drug deposited on the surface and adhered the particles to one another. In the physisorption measurements, the Zn MOF-74 samples decreased in surface area with ibuprofen loading, until they became zero at 80 wt%. In UTSA-74, the drug impregnation was less effective, as 35% of the original surface area was retained in the 80 wt% sample. On the basis of our drug release measurements, 50 wt% ibuprofen loading was found to be optimal on Zn MOF-74, as it gave rise to fast kinetics ($k = 0.27\ h^{-1/2}$) and high drug concentrations within the first 10 h. In UTSA-74, the fastest release rate was observed at 30 wt% loading ($k = 0.22\ h^{-1/2}$), as the poor impregnation efficiency blocked diffusion through the MOF pores at higher loading. Color changes of phosphate buffer saline (PBS) solutions at different time intervals also suggested that Zn MOF-74 decomposed during drug release, as it produced yellowing of the PBS solution. On the other hand, UTSA-74 did not discolor the PBS solution, and was concluded to not have dissolved during drug release. From these results, it was concluded that Zn MOF-74 was the superior drug carrier, as it could effectively deliver higher ibuprofen loadings and would dissolve in the process of drug release, thereby reducing its invasiveness in the human body.

1. Introduction

Traditionally, medicinal drugs have been delivered through encapsulation inside of tablets alongside innocuous binding agents [1–3]. While this method is effective for delivering low dosages of an administered drug, encapsulation becomes far less effective at elevated concentrations because increasing the drug loading also increases the capsule size, which can lead to difficulty swallowing. Moreover, digestion of the inert binder leads to a "burst" of drug release, rather than a controlled dissolution [4], which can produce undesirable side effects including incomplete drug permeation into the cell wall, nausea, and liver necrosis [5]. Therefore, controlling the release rate for administered drugs – especially at elevated dosages – is one of the biggest challenges in modern medicine.

In recent years, one way of delivering high drug concentrations while still controlling the dissolution rate has been through immobilization onto nanoporous materials such as zeolites [6,7], activated carbon [8,9], and metal-organic frameworks (MOFs) [10–12]. Of these materials, MOFs are especially promising for drug delivery applications because their sizable surface areas and pore volumes can incorporate high concentrations of impregnated compounds and their textural properties can be easily tuned by varying the solvothermal growth conditions, which allows for precise control of the drug release rate. For example Horcajada et al. [10] was able to impregnate up to 50 wt% of ibuprofen onto MIL-100 (Cr) and MIL-101 (Cr) and observed 70% total release within 24 h. Similar works have also explored Nu-1000 (Zr) [12,13], UIO-66-NH_2 (Zr) [14,15], and HKUST-1 (Cu) [11,16,17] MOFs for the release of alpha- cyano-4-hydroxycinnamic acid, ibuprofen, and 5-fluoracil, and more. Of these MOFs, Nu-1000, which has a mesoporous diameter, achieved the highest drug loading (80 wt%) compared to the other samples and is considered one of the best drug delivery platforms to date, especially since it exhibited nearly zero reductions in release kinetics at the highest drug loading [12]. Nevertheless, it should be noted here that Nu-1000 synthesis is

* Corresponding author.
E-mail address: rezaeif@mst.edu (F. Rezaei).

https://doi.org/10.1016/j.msec.2020.111336
Received 14 May 2020; Received in revised form 6 July 2020; Accepted 30 July 2020
Available online 07 August 2020
0928-4931/

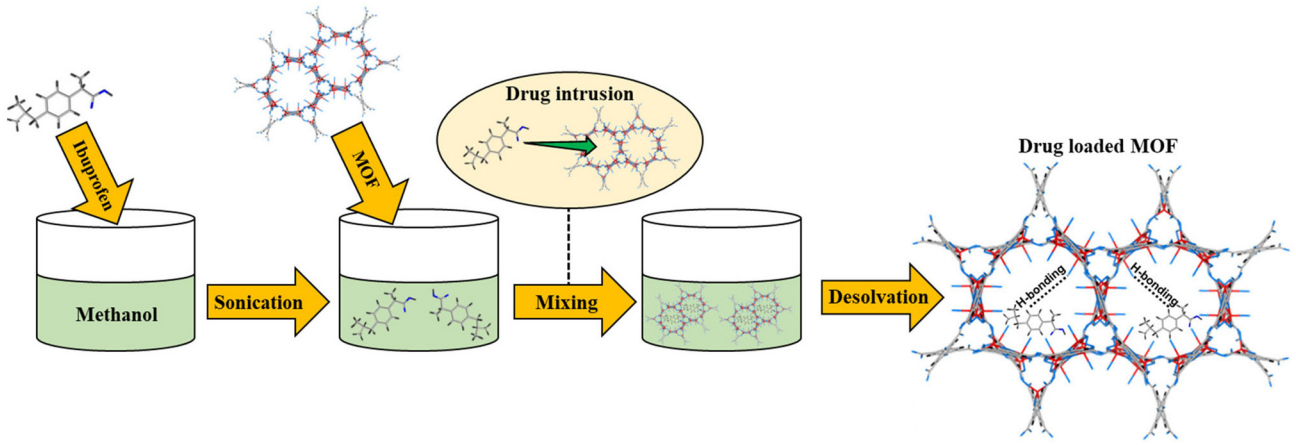

Fig. 1. Schematic representation of drug loading on MOF by the wet impregnation method.

extremely time consuming – being comprised of thirty steps – and is quite hazardous, on account of its chloroform and dioxane use [18]. For these reasons, Nu-1000 cannot be justified as a scaled-up drug carrier and alternative MOFs should be explored.

For effective drug delivery, the MOF should contain both a mesoporous pore diameter – to maximize effective drug loading and ensure rapid release rate – as well as metal centers which exist in the everyday diet (Cu, Mg, Fe, or Zn) to minimize invasiveness in the human body. Additionally, the MOF synthesis should also not be overly complex in order to be effective for scale-up. Fitting these criteria, the mesoporous MOFs Zn MOF-74 [19], and its pore-expanded variant UTSA-74 [20], are worth considering as potential drug carriers, as they are both comprised of Zn which is of low toxicity [21], contain mesoporous pore diameters, and are formed in a high-yield one pot synthesis. Of such benefits, these MOFs' metal centers and simple solvothermal synthesis procedures make them attractive drug delivery platforms, as synthesizing the MOFs can be accomplished in single large batches in less than one week, while the Zn metal centers meet the biocompatibility criteria, as they already exist in dietary sources. Also worth noting, reports of MOFs as drug delivery platforms with biocompatible metal centers are scarce and, in this regard, it is worth expanding this area of research to include new materials. To the best of our knowledge, these MOFs have not yet been investigated as drug carriers and, based on these desirable properties, we embarked on a study which investigates them as biocompatible platforms for drug delivery.

In this work, we investigated Zn MOF-74 and UTSA-74 for the delivery of ibuprofen in phosphate buffer saline (PBS) solution. Ibuprofen was selected as a proof-of-concept because of its similarity to other drugs and previous investigation on MOF materials. To be more specific, ibuprofen has been extensively studied on MOFs such as MIL-101, UIO-66, Cu-terephthalate, and others to assess their pharmacokinetics, since it is an over-the-counter painkiller and its quick absorption into the body is one of its most important properties [10,14,22–25]. Both MOFs were impregnated with 30, 50, and 80 wt% ibuprofen loadings to study the effect of drug concentration on release rate and to determine the maximum effective loading for each MOF. The samples were characterized by X-ray diffraction (XRD), scanning electron microscopy (SEM), and N_2 physisorption. The rates of drug release were measured by high performance liquid chromatography (HPLC) to determine the MOFs' efficacy for ibuprofen delivery. Overall, this work establishes two biocompatible mesoporous MOFs for ibuprofen delivery which could likely be used as drug carriers for other compounds.

2. Experimental section

2.1. Materials

The following materials were purchased from Sigma-Aldrich and were used for MOF synthesis and ibuprofen delivery experiments: 2,5 Dihydroxyterephthalic acid (98%), $Zn(NO_3)_2.6H_2O$ (98%), and ibuprofen (98%). The following solvents and buffers were also used: acetonitrile (HPLC), distilled water (HPLC), phosphate buffer saline (PBS, pH = 7.4), Na_2HPO_4 (98%), *N,N*-dimethylformamide (DMF, ACS), and MeOH (ACS). The Na_2HPO_4 was dissolved in HPLC grade water to make a 10 mM solution for HPLC experiments. All other reagents were used without modification.

2.2. MOF synthesis and ibuprofen impregnation

Zn MOF-74 and UTSA-74 were synthesized using their established procedures [19,20]. Here, it should be noted that the literary activation procedure for UTSA-74 was not specified in the reported synthesis. Therefore, we applied the Zn MOF-74 activation procedure to UTSA-74. Specifically, UTSA-74 was washed for 72 h in MeOH at room temperature, where the solvent was exchanged every 24 h, followed by activation under vacuum at 158 °C for 12 h. Here, we suggest that it might be advantageous to vary the solvent used for UTSA-74 activation, as this could give rise to differences in MOF pore structure and enhanced pharmacokinetics, however, this should be the focus of a later study. Ibuprofen was loaded by the wet-impregnation technique, as shown in Fig. 1. This was accomplished by first dissolving the desired amount of ibuprofen in 10 mL MeOH/0.05 g ibuprofen via sonication at 25 °C for 10 min. Then, 0.5 g of MOF was added to the flask. The suspension was sealed with a septum and stirred at 350 rpm for 24 h at room temperature. Finally, the MeOH was extracted via rotary evaporation at 70 °C for 15 min under vacuum. Using this method, the MOFs were impregnated with 30, 50, and 80 wt% ibuprofen. The Zn MOF-74 samples are noted as Zn MOF-74, Zn MOF-74 (30), Zn MOF-74 (50), and Zn MOF-74 (80), respectively, while the UTSA-74 samples are denoted as UTSA-74, UTSA-74 (30), UTSA-74 (50), and UTSA-74 (80), respectively.

2.3. Materials characterization

The samples' textural properties were evaluated by N_2 physisorption at 77 K on a Micromeritics (3Flex) gas analyzer. The surface areas were calculated by the Brunauer-Emmet-Teller (BET) method and the pore volumes were calculated using the nonlocal density functional theory (NLDFT) method. Prior to analysis, the samples were degassed under vacuum at 158 °C for 6 h on a Micromeritics Smart VacPrep system. The

pristine MOFs and 50 wt% ibuprofen samples' crystallinities were assessed by X-ray diffraction (XRD) on a PANalytical X'Pert multipurpose X-ray diffractometer with a scan step size of 0.02°/step at the rate of 137.2 s/step. The 50 wt% samples' crystallinities were also assessed by XRD after drug delivery experiments to determine any changes in structure caused by PBS exposure. The MOFs' topologies at different degrees of drug loadings were assessed by scanning electron microscopy (SEM) using a Zeiss Merlin Gemini field emission SEM (FE-SEM).

2.4. Drug release experiments

PBS was used as an analogue for human body fluid in the drug delivery experiments. The experiments were carried out in 200 mL PTFE bottles. Prior to the delivery experiments, the bottles were sterilized with dilute hydrofluoric acid for 12 h to eliminate any contaminants. After washing, the bottles were rinsed with distilled water and dried in a vacuum oven at 50 °C for 12 h. In the drug release experiments, 100 mL of PBS was heated to 37 °C for 1 h to simulate human body temperature. Before adding the MOF, a 0.5 mL sample was collected and labeled as 0 h. Then, 0.05 g (impregnated weight) of the MOF was added to the PBS and 0.5 mL samples were taken every hour for 1–10 h as well as at the 24 h mark. Prior to loading the sample into the HPLC vial, the solution was passed through a 2 μm filter to remove any particulate matter. The MOFs' drug delivery performances were measured by HPLC on an Agilent 1260 Infinity II HPLC using a procedure established by Han et al. [26] for ibuprofen detection. In our system, the C18 column dimensions were 4.6 × 100 mm and the detection time was 10 min. Otherwise, the method was identical to the reference material. The normalized profiles from HPLC were fitted using the Higuchi technique which has been detailed previously (Eq. (1)): [27]

$$a = kt^{\frac{1}{2}} \tag{1}$$

where a is the normalized quantity of drug released, k is the release rate constant ($h^{-1/2}$), and t is the elapsed time (h). Using the data gathered from HPLC, the release rate constant was varied to maximize the R^2 value. Here, it should be noted that the Higuchi technique was selected to model our drug delivery rates because its assumptions with regards to overall diffusion refer to molecular release from a planar system with a pore matrix, such as MOFs, as detailed in the literature [27].

3. Results and discussion

3.1. Materials characterization

The samples' N_2 physisorption isotherms and NLDFT pore distributions are shown in Fig. 2, while the corresponding textural properties are contained in Table 1. As was expected, increasing the drug loading decreased the N_2 physisorption capacity and pore volume in both MOFs. This was especially true in Zn MOF-74 (80) (Fig. 2a), as the high drug loading completely saturated the MOF surface and led to a complete loss in N_2 physisorption capacity and pore volume (Fig. 2c). On the other hand, UTSA-74's less efficient loading caused it to retain most of the physisorption capacity (Fig. 2b) and a sizable portion of the pore volume (Fig. 2d), even at 80 wt% impregnation. It is also worth noting here that, with the exception of UTSA-74 (80) who exhibited type IV (a) physisorption behavior with type-H3 hysteresis and corresponds to aggregated particles [28], all samples examined in this study exhibited nearly linear physisorption isotherm profiles with only slight hysteresis. Importantly, the physisorption shapes were not consistent with any of the IUPAC classifications, however, they were most similar to Type IV behavior, which is indicative of multilayer capillary condensation within mesoporous materials [28] and agrees with the MOFs' respective literature [19,20]. In fact, when magnifying the low and high pressure ends of the isotherms, slight knees could be observed, which further indicated Type IV behavior because, at lower pressure, there was not sufficient capillary action to produce condensation within the mesopores, whereas, at higher pressure, the elevated force gradient led to increased condensation within the large pore diameters. This conclusion was further supported by the pore size distributions, as pore diameters of 3, 8.5, and 13 nm were observed for the pristine Zn MOF-74 (Fig. 2c) while slightly larger diameters of and diameters of 3, 5, 13.5, and 17 nm were observed for UTSA-74 (Fig. 2d). More importantly, the pore volumes were found to decrease steadily for both MOFs at higher drug loading, where 80 wt% ibuprofen loading in Zn MOF-74 produced an entirely nonporous material. In UTSA-74, on the other hand, the pristine MOFs' initial pore volume was higher than that of Zn MOF-74 and some of the open sites remained unblocked at the higher drug loading.

The samples' textural properties are contained in Table 1. In the bare MOFs, the surface areas and pore volumes were both consistent with established literature [19,20] which further indicated that they were synthesized properly. Upon loading 30 wt% ibuprofen, Zn MOF-74 exhibited a 32% reduction in surface area and 22% reduction in pore volume. Meanwhile, loading the same amount of ibuprofen on UTSA-74 decreased its surface area by 6% and its pore volume by 9% suggesting that the loading was less efficient on UTSA-74 compared to Zn MOF-74. At 50 and 80% loadings, the differences between the two MOFs were further evident, as Zn MOF-74 continued to exhibit losses in surface area and pore volume while the UTSA-74 samples retained most of their pore volume but experienced losses in surface area. Effectively, this indicated that ibuprofen loading was more allocated to the surface on UTSA-74, while the drug intruded the pores in Zn MOF-74.

The SEM micrographs for the pristine and drug loaded MOFs are shown in Fig. 3. As can be seen, the pristine Zn MOF-74 particles (Fig. 3a) exhibited a spherical topography with diameters ranging from 300 nm–3 μm. The crystal structure and particle diameter were in agreement with the MOF's literature [19], indicating that it had been synthesized successfully. At 30 wt% ibuprofen loading (Fig. 3b), Zn MOF-74 retained its particle size and structure, however, the particles were slightly more agglomerated compared to the pristine MOF. This result agreed with the textural properties in Table 1, which showed only a marginal decrease in pore volume from the pristine MOF to the 30 wt % ibuprofen sample. On the other hand, when the loading was increased to 50 wt% (Fig. 3c), the Zn MOF-74 particles began to lose their distinctive topographical structures, indicating that the drug had mostly saturated the pore windows and began loading on the MOF surface. Once again, this agreed with the textural properties, which showed a sizable reduction in pore volume from 30 to 50 wt% ibuprofen loading. Finally, the 80 wt% ibuprofen sample (Fig. 3d) showed no identifiable crystal faces or particles, effectively indicating that the drug had completely coated the MOF surface.

In UTSA-74, the pristine MOF exhibited a biphasic distribution, where both spherical nanoparticles and large cubic structures were observed (Fig. 3e). The presence of these smaller nanoparticles likely could be attributed to differences in cooling rate between our synthesis and the original method. Namely, because we scaled-up the original synthesis to produce enough MOF for impregnation, a 125 mL autoclave was used instead of the 12 mL reported in literature. Because our autoclave was considerably larger, the cooling rate could have been slower than the original 0.1 °C/min. Consequently, this may have led to additional precipitation of smaller particulate. This being stated, because the larger cubic phase was consistent with literary SEM images for UTSA-74, this MOF was still considered for drug delivery. Moreover, because we identified this phase as that of UTSA-74 from literature, the SEM images are focused on the effects of drug loading for that phase. As can be seen, loading 30 wt% of ibuprofen onto UTSA-74 led to agglomeration of the small particles on the MOF surface, however, the overall cubic structure was still retained (Fig. 3f). Notably, this result differed from that for the Zn MOF-74 (30) sample, which exhibited only slight agglomeration, and suggested that the drug loading was more allocated to the UTSA-74 surface instead of the pores. This effect

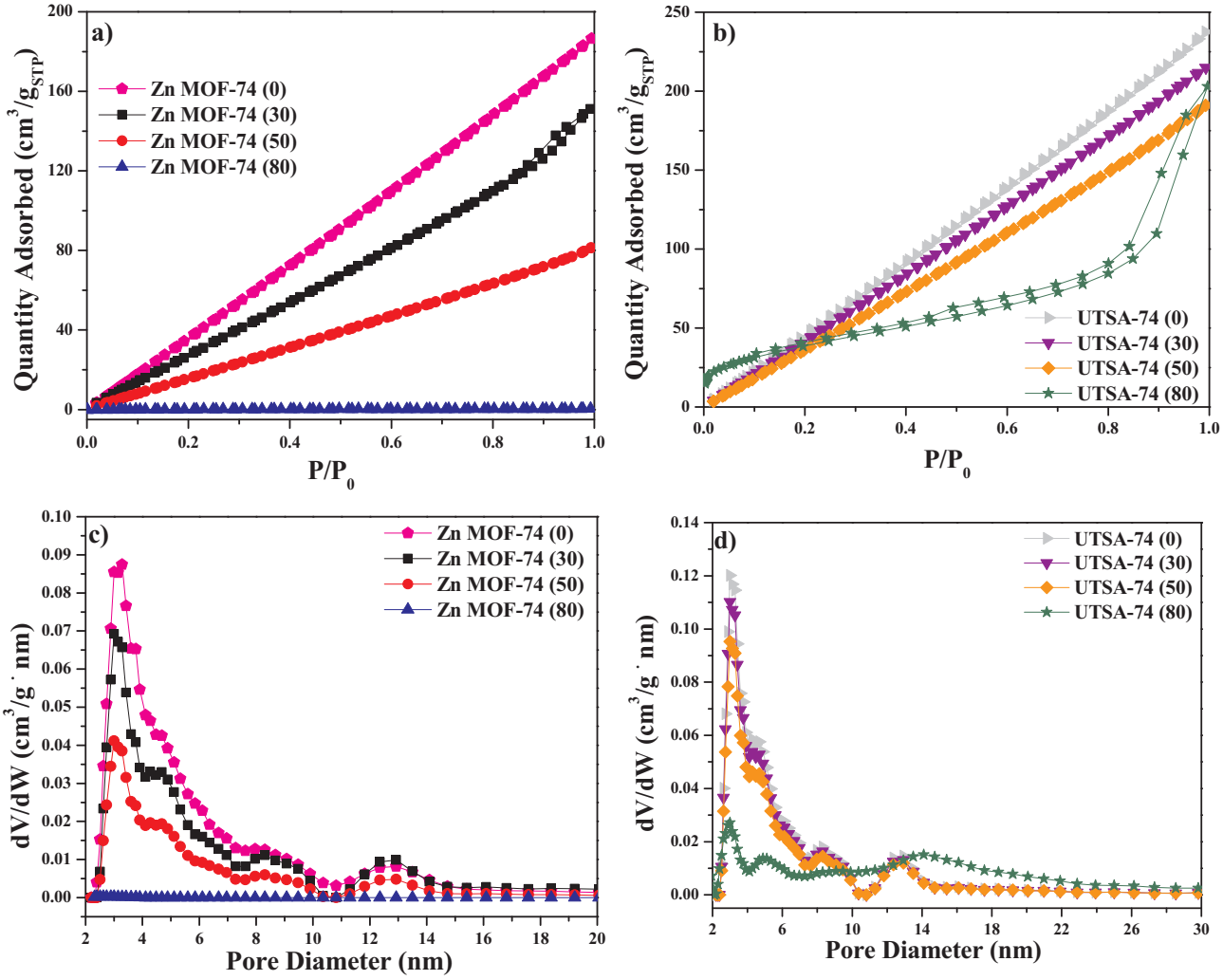

Fig. 2. (a–b) N_2 physisorption isotherms and (c–d) NLDFT pore distributions for Zn MOF-74 and UTSA-74 samples.

Table 1
Textural properties of drug carrier Zn-MOFs.

Sample	S_{BET} (m^2/g)	$V_{p\text{-micro}}$ (cm^3/g)	$V_{p\text{-}meso}$ (cm^3/g)	Pore diameter (nm)
Zn MOF-74 (0)	320	0.00	0.27	3, 8.5, 13
Zn MOF-74 (30)	220	0.00	0.22	3, 5, 8.5, 13
Zn MOF-74 (50)	130	0.00	0.12	3, 5, 8.5, 13
Zn MOF-74 (80)	2	0.00	0.00	–
UTSA-74 (0)	403	0.00	0.35	3, 5, 7, 13.5
UTSA-74 (30)	379	0.00	0.32	3, 5, 7, 13.5
UTSA-74 (50)	323	0.00	0.28	3, 5, 7, 13.5
UTSA-74 (80)	143	0.00	0.28	3, 5, 7, 14.0

became further pronounced at 50 wt% ibuprofen loading (Fig. 3g), where the MOF exhibited a smoother topography with fewer defined crystal phases. Unlike UTSA-74 (30), who exhibited differing changes particle agglomeration compared to Zn MOF-74 (30), this result was comparable to the one observed for Zn MOF-74 (50), which also exhibited losses in particle definition. Finally, UTSA-74 (80) experienced complete and total losses in the crystalline structure and severe agglomeration of particles, indicating that the drug had completely saturated the MOF surface.

The observed ibuprofen loading behavior can be explained by the mechanism shown in Fig. 4. Beginning with the pristine MOF, oxygen free radicals are present within the MOF pore, where they are covalently bound to the metal center, as well as on the outside shell, where they are covalently bound to the organic linker carbon chains. These free radicals are created during MOF activation, where removal of guest solvents (DMF, water, alcohols, etc.) from the MOF structure frees up valence electron pairs in the oxygen species. As was postulated by Ahmed and Jhung [29], these free electrons play in important role in adhering functional groups (aminopolymers, ibuprofen, etc.) because they produce hydrogen bonding with the guest species upon impregnation. At low guest loadings (i.e. 30 wt% ibuprofen), the intermolecular bonding first occurs within the MOF pores, as the higher concentration of free radicals enhances the electrostatic attraction between the drug's positive hydrogen and the MOF's negative oxygen [30], similar to the interactions with adsorbed H_2O [31]. At this stage, the MOF particles do not exhibit any differences in topography, as the drug is encapsulated inside of the structure and does not promote agglomeration between particles. Upon increasing the loading to 50 wt% ibuprofen, however, the MOF pore becomes completely saturated with ibuprofen and the drug begins to interact with the less plentiful surface oxygens. As was observed in the SEM images, this leads to slight agglomeration of MOF particles, as the surface-loaded ibuprofen is no longer isolated inside of the pores and, therefore, can produce hydrogen bonding with multiple interfaces. Nevertheless, this effect is relatively marginal at 50 wt% ibuprofen loading, as the drug barely begins to saturate the MOF surface. On the other hand, at 80 wt% loading the MOF surface becomes fully saturated with the drug. This causes the ibuprofen to deposit on top of itself because the only accessible electrons are contained within the drugs' carboxylic acid centers [30].

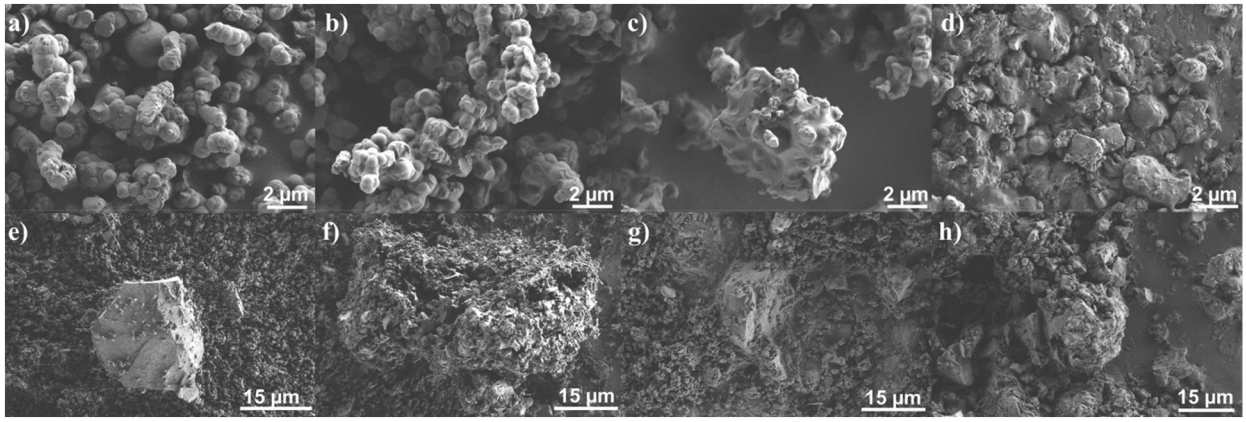

Fig. 3. SEM micrographs of (a) pristine Zn MOF-74, (b) Zn MOF-74 (30), (c) Zn MOF-74 (50), (d) Zn MOF-74 (80), (e) pristine UTSA-74, (f) UTSA-74 (30), (g) UTSA-74 (50), and (h) UTSA-74 (80).

Accordingly, this causes hydrogen bonding to occur between individual ibuprofen molecules, thereby leading to further particle agglomeration and poor performance in drug delivery applications.

3.2. Drug release experiments

The ibuprofen concentrations and normalized drug release rates from HPLC experiments are shown in Fig. 5. Ibuprofen was detected at ~6 min which was in agreement with literature [26]. From the calculated peak areas, Zn MOF-74 (Fig. 5a) was able to deliver 50% more ibuprofen at 50 wt% loading and 45% more ibuprofen at 80 wt% loading compared to UTSA-74 (Fig. 5b). This was attributed to the latter's less efficient drug loading at elevated ibuprofen concentrations, which was consistent with the N_2 physisorption measurements and textural properties. At 30 wt% ibuprofen, however, UTSA-74 delivered ~50% more drug than Zn MOF-74. Likely, this could have been a result of the former's larger pore diameters, which allowed for a more complete release of the drug. On the other hand, Zn MOF-74's smaller pore diameter likely slowed ibuprofen diffusion from the pores slightly and caused partial ibuprofen retention. This was further evidenced by differences between the samples' normalized release rates, where Zn MOF-74 (30) (Fig. 5c) exhibited a broader concentration profile than UTSA-74 (30) (Fig. 5d). At 50 wt% ibuprofen loading, however, the opposite trend was observed. Namely, Zn MOF-74 (50) released its ibuprofen much faster than UTSA-74 (50). Quite likely, this could be attributed to Zn MOF-74 (50)'s more efficient loading within the MOF pores compared to UTSA-74 (50), which was first observed in the textural properties, and may have been caused by incomplete activation of the UTSA-74 structure. This being stated, 50 wt% was concluded to be the maximum effective ibuprofen loading for both MOFs, as further increasing the drug loading to 80 wt% dramatically broadened the release kinetics and caused incomplete dissolution of the administered compound in both samples.

The normalized drug releases were fitted using a technique detailed by previously. The fitted HPLC profiles are shown in Fig. 6 while the calculated release rate constants are displayed in Table 2. As can be seen, the R^2 values for all six simulated fittings were greater than 0.9, indicating that the selected model was appropriate for the datasets. This was especially true for Zn MOF-74 (30) (Fig. 6a), Zn MOF-74 (50) (Fig. 6b) and UTSA-74 (30) (Fig. 6d), where the simulated model was nearly identical to the curve fitting. This likely signified that, for those three samples, the ibuprofen diffusion occurred from the pore to the PBS solution, as this particular mechanism is the driving force in the Higuchi model that was used here. However, in Zn MOF-74 (80) (Fig. 6c), UTSA-74 (50) (Fig. 6e), and UTSA-74 (80) (Fig. 6f), the model was not as good of a fit. This likely was caused by the drug diffusing from the nanoparticulate surface into the PBS, rather than diffusing from the pore. More specifically, this was attributed to a decreased amount of drug surface area exposed to the PBS, on account of the layer-wise deposition on the MOFs' surfaces and the observed agglomeration of MOF particles. In turn, this led to a multifaceted diffusion mechanism where part of the dissolution rate was dependent on the ibuprofen solubility while another portion was dependent on the amount of exposed MOF surface area. This was further evidenced by the

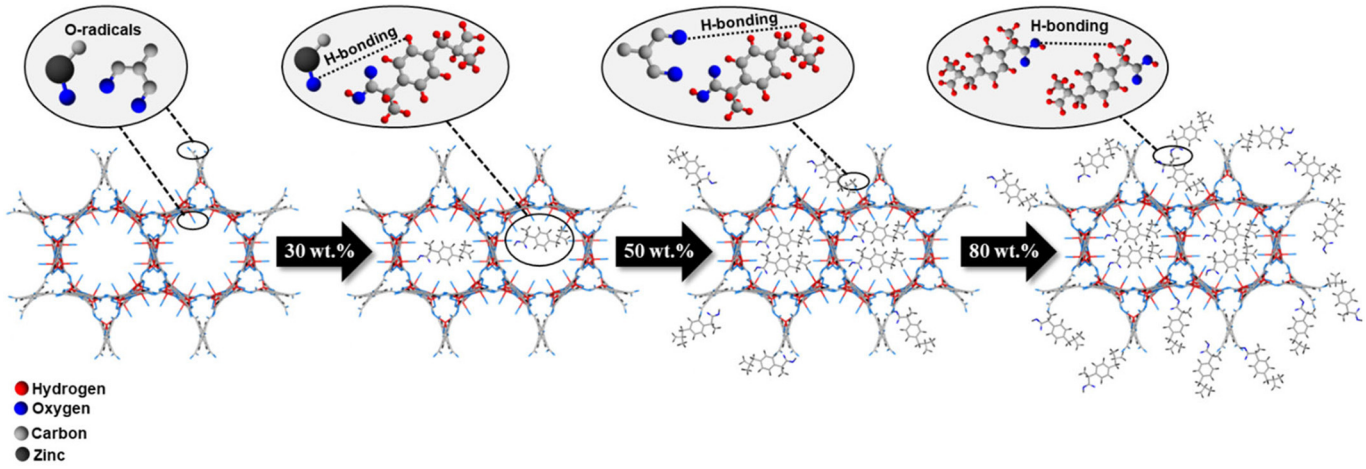

Fig. 4. Schematic representation of ibuprofen loading mechanism within MOF structure.

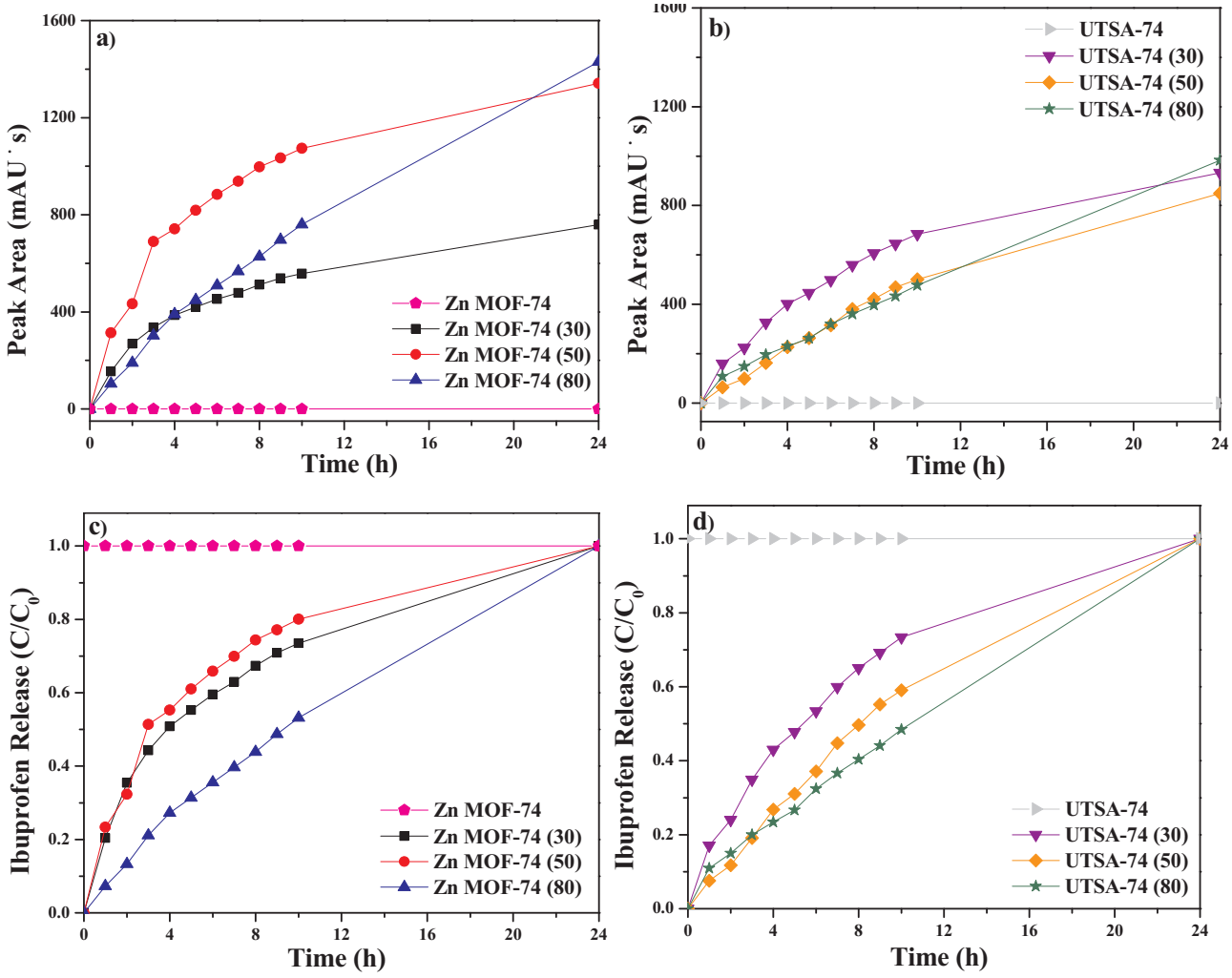

Fig. 5. (a–b) Ibuprofen peak concentrations and (c–d) normalized release rates for Zn MOF-74 and UTSA-74 in PBS at 37 °C from 0 to 10 and 24 h.

SEM images, which clearly showed ibuprofen deposition on the MOF surfaces at higher loadings, and caused the release rates to be less accurately represented by the Higuchi model for Zn MOF-74 (80), UTSA-74 (50), and UTSA-74 (80). Nevertheless, because the R^2 values were all greater than 0.90, the data was considered to be accurately represented by the Higuchi model.

The release rate constants were varied to achieve the curve fittings in Fig. 6 and are displayed in Table 2. As can be seen, Zn MOF-74 (30) and Zn MOF-74 (50) achieved nearly identical release rate constants, which indicated that these two samples had the least amount of diffusional resistance caused by surface loading of the drug. On the other hand, a ~50% reduction in the release rate constant was observed in Zn MOF-74 (80), which could be attributed the surface loading and particle agglomeration that was observed in the SEM images. More specifically, the surface ibuprofen loading and particle agglomeration blocked some of the MOF pores, thereby imparting resistance to dissolution, and slowing drug release. This further signified that 50 wt% was the maximal effective ibuprofen loading on Zn MOF-74, as further increasing the drug concentration led to a dramatic reduction in pharmacokinetics.

In UTSA-74, the fastest release rate constant was observed in the 30 wt% ibuprofen sample. Notably, this release rate was comparable to that for Zn MOF-74 (30) and Zn MOF-74 (50) samples, signifying that UTSA-74 can be used to rapidly deliver small amounts of ibuprofen. However, as the drug loading was increased to 50 wt%, UTSA-74 exhibited a 33% reduction in the release rate constant. A similar loss of 34% was also observed upon increasing the loading from 50 to 80 wt%. As with the Zn MOF-74 (80) sample, these losses in release rate constant were attributed to the surface drug loading and particle agglomeration blocking some of the accessible pores. From these results, the maximal effective loading for UTSA-74 was definitively determined to be 30 wt% ibuprofen, as the agglomeration of particles at higher loadings rendered UTSA-74 an ineffective drug carrier. Because of this, Zn MOF-74 was concluded to be the better carrier for ibuprofen, as it can balance fast kinetics with elevated drug loadings. Moreover, it is also worth noting here that the release rate constants for ibuprofen on Zn MOF-74 (50) and Zn MOF-74 (30) were substantially higher than other benchmark MOFs for ibuprofen, such as MIL-100 (k = 0.21 $h^{-1/2}$, ibuprofen loading = 25.5 wt%) or UIO-66 (k = 0.11 $h^{-1/2}$, ibuprofen loading = 25.5 wt%) [32], indicating that this MOF is a superior drug carrier, as it can deliver a greater drug concentration at a more dynamic rate. Quite possibly, this could be attributed to the superior solubility of Zn clusters compared to Zr or Cr, which allow the MOF structure to decompose during release and rapidly administer the drug. Even in UTSA-74 (30), where the release rate constant was lower compared to Zn MOF-74 (30) and Zn MOF-74 (50), it still achieved a similar release rate constant to MIL-100 and double the release rate constant of UIO-66 with 5 wt% more ibuprofen. For this reason, UTSA-74 is also worth considering for drug delivery applications, as it can load a comparable amount of drug to current benchmarks and release said drug at an acceptably fast rate.

The samples' XRD patterns are shown in Fig. 7. As evident, the

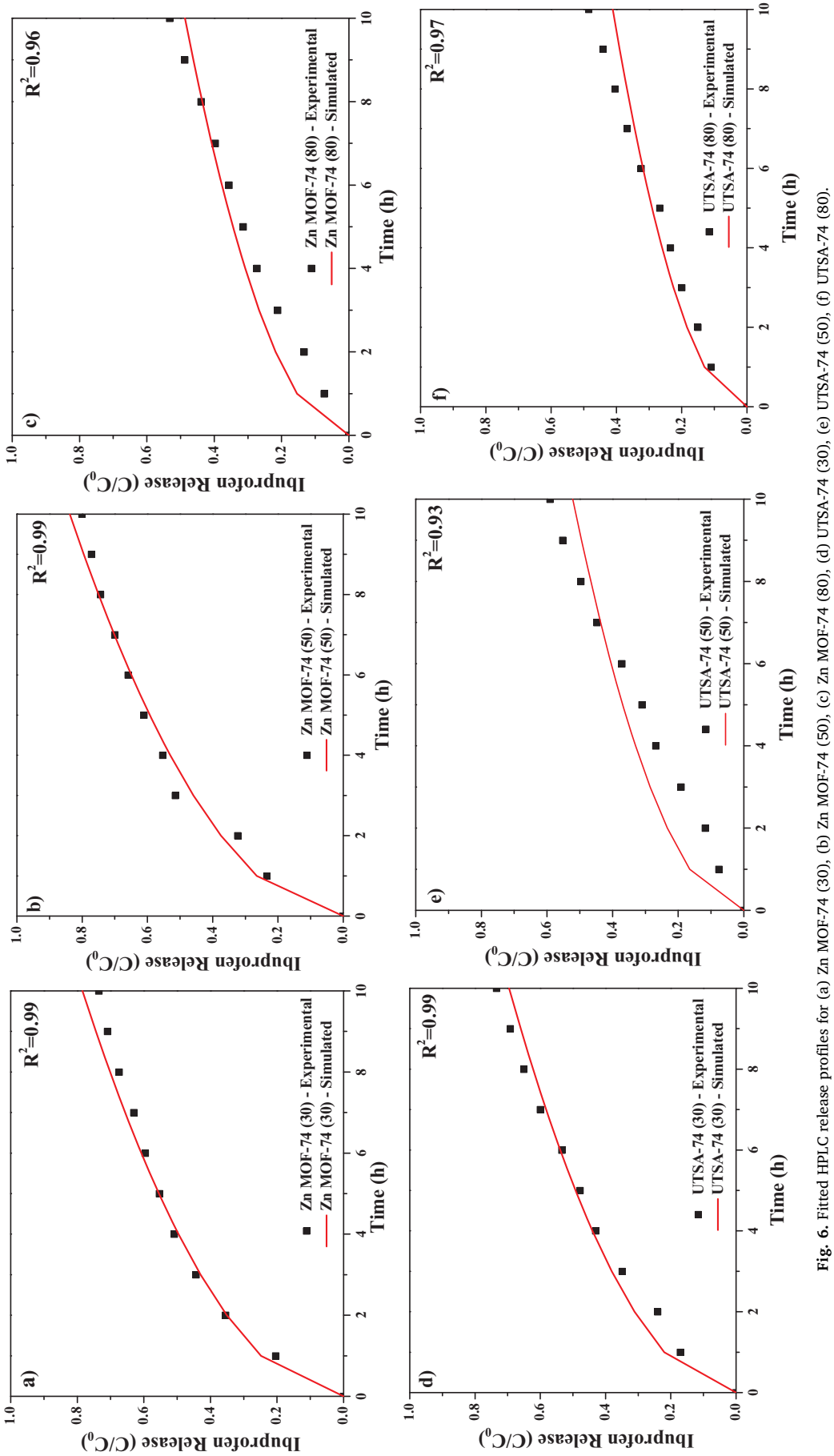

Fig. 6. Fitted HPLC release profiles for (a) Zn MOF-74 (30), (b) Zn MOF-74 (50), (c) Zn MOF-74 (80), (d) UTSA-74 (30), (e) UTSA-74 (50), (f) UTSA-74 (80).

Table 2
Ibuprofen release rate constants estimated from Higuchi model.

Sample	k ($h^{-1/2}$)
Zn MOF-74 (30)	0.25
Zn MOF-74 (50)	0.27
Zn MOF-74 (80)	0.15
UTSA-74 (30)	0.22
UTSA-74 (50)	0.17
UTSA-74 (80)	0.13

synthesized Zn MOF-74 (Fig. 7a) exhibited diffractive patterns which were consistent with literary reports [19]. However, after ibuprofen loading, the diffractive indices could no longer be seen. This was to be expected from the SEM images, which indicated that the crystalline faces became obscured at 50 wt% ibuprofen loading. Moving onto UTSA-74 (Fig. 7b), the MOFs major diffractive peaks at $2\theta = 5$, 7.5, 14.5, 16, 19, and 27.5° were detected, which signified that the MOF had been formed successfully [20]. This being the case, it is important to note here that, because the MOF was the less dominant phase, as observed in SEM, the signal had to be magnified from $5° \leq 2\theta \leq 30°$ in order to view the MOFs' diffractive indices because the other phase produced strong peaks at $2\theta > 30°$ which were of much greater intensity. Nevertheless, the major peaks were still detected and, for this reason, the MOF was still considered for ibuprofen delivery. Upon 50 wt % impregnation, UTSA-74 experienced a complete loss in its diffractive indices, indicating that it too had become saturated with the drug. Again, this result was to be expected from the SEM images, which signified that UTSA-74 exhibited an amorphous topography and agglomerated particles when the ibuprofen loading was 50 wt% or more. This was also consistent with literary reports for other MOFs, which show substantial losses in crystallinity when the drug loading is increased beyond 50 wt% [22,23,33,34]. Because of this, it was impossible to determine from XRD if the MOF decomposed during PBS exposure, and other characterizations were used to examine the aqueous stability.

Because differences in MOF decomposition could not be determined from the XRD patterns, we also took optical photographs of the 50 wt% ibuprofen samples' HPLC vials from 0 to 10 and 24 h, as shown in Fig. 8, to illustrate differences in the solutions' discolorations. As can be seen, Zn MOF-74 (50) (Fig. 8a) produced a lightly brown solution that got darker over time while UTSA-74 (50) (Fig. 8b) produced a clear solution, with only slight discoloration at the 24 h mark. Notably, ibuprofen

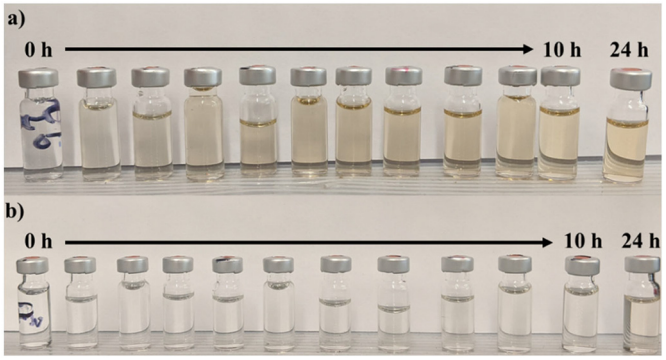

Fig. 8. Optical photographs of HPLC vials taken from (a) Zn MOF-74 (50) and (b) UTSA-74 (50) from 0 to 10 h and 24 h.

is not known to produce a color change when in solution [35] and, therefore, the differences in sample color could likely be attributed to decomposition of the MOF centers. Specifically, the slight yellow-brown color typically coincides with the presence of organic moieties in water, likely indicating that Zn MOF-74 (50) decomposed while UTSA-74 (50) remained stable. Given that MOF decomposition is an important property for drug delivery, because it minimizes the retention time in the digestive track, the photographs in Fig. 8 suggested that Zn MOF-74 could be a superior drug carrier compared to UTSA-74 from a biocompatibility perspective.

4. Conclusions

In this work, we examined two new biocompatible MOFs (Zn MOF-74 and UTSA-74) for ibuprofen delivery. Between the two MOFs, the ibuprofen loading was more effective in Zn MOF-74 compared to UTSA-74, as the former's structure experienced more complete activation and could deliver a higher ibuprofen concentration (50 vs. 30 wt%, respectively) at a faster rate (0.27 vs. 0.22 $h^{-1/2}$, respectively). In UTSA-74, however, the poorly defined activation procedure likely caused a fraction of the drug to load on the surface, leading to slow release rate and increased particle agglomeration. UTSA-74 also exhibited increased stability during the drug delivery experiments, which would increase its retention time after consumption, and decrease its biocompatibility. Accordingly, Zn MOF-74 was concluded to be the superior biocompatible MOF for drug delivery, as it was capable of delivering more ibuprofen at a faster rate and appeared to have dissociated within 24 h. This being stated, both of the MOFs examined in this study were able to

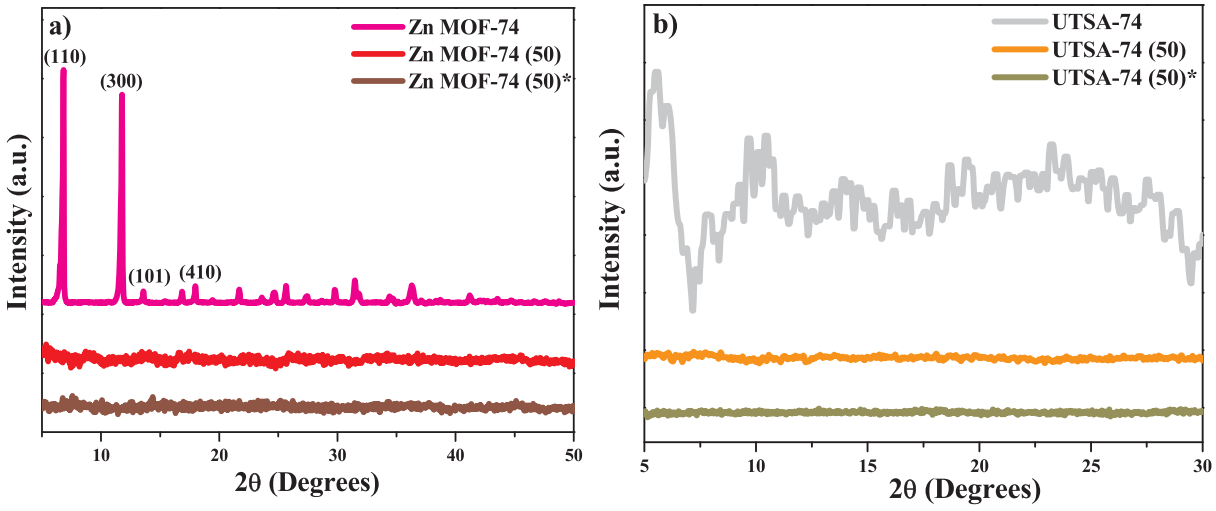

Fig. 7. XRD patterns for (a) Zn MOF-74 and (b) UTSA-74 samples. (*) indicates after drug release experiments.

successfully act as ibuprofen carriers and may be considered potential biocompatible platforms for drug delivery.

Declaration of competing interest

The authors of this manuscript declare no competing financial interest.

Acknowledgements

The involvement of Shane Lawson in this work was sponsored by the National Science Foundation internship program (NSF CBET-1802049). The authors would like to acknowledge Oak Ridge National Laboratories (ORNL) for allowing us to use their SEM and XRD facilities.

References

[1] R.P. Chitemere, S. Stafslien, B. Rasulev, D.C. Webster, M. Quadir, Soysome: a surfactant-free, fully biobased, self-assembled platform for nanoscale drug delivery applications, ACS Appl Bio Mater. 1 (2018) 1830–1841, https://doi.org/10.1021/acsabm.8b00317.

[2] S. Roy, N.M. Elbaz, W.J. Parak, N. Feliu, Biodegradable alginate polyelectrolyte capsules as plausible biocompatible delivery carriers, ACS Appl Bio Mater. 2 (2019) 3245–3256, https://doi.org/10.1021/acsabm.9b00203.

[3] S.V. Sastry, J.R. Nyshadham, J.A. Fix, Recent technological advances in oral drug delivery - a review, Pharm Sci Technol Today. 3 (2000) 138–145, https://doi.org/10.1016/S1461-5347(00)00247-9.

[4] P. Horcajada, T. Chalati, C. Serre, B. Gillet, C. Sebrie, T. Baati, J.F. Eubank, D. Heurtaux, P. Clayette, C. Kreuz, J.S. Chang, Y.K. Hwang, V. Marsaud, P.N. Bories, L. Cynober, S. Gil, G. Férey, P. Couvreur, R. Gref, Porous metal-organic-framework nanoscale carriers as a potential platform for drug deliveryand imaging, Nat. Mater. 9 (2010) 172–178, https://doi.org/10.1038/nmat2608.

[5] M. Saravanan, K. Bhaskar, G. Srinivasa Rao, M.D. Dhanaraju, Ibuprofen-loaded ethylcellulose/polystyrene microspheres: an approach to get prolonged drug release with reduced burst effect and low ethylcellulose content, J. Microencapsul. 20 (2003) 289–302, https://doi.org/10.1080/0265204031000093087.

[6] R. Amorim, N. Vilaça, O. Martinho, R.M. Reis, M. Sardo, J. Rocha, A.M. Fonseca, F. Baltazar, I.C. Neves, Zeolite structures loading with an anticancer compound as drug delivery systems, J. Phys. Chem. C 116 (2012) 25642–25650, https://doi.org/10.1021/jp3093868.

[7] Y.P. Guo, T. Long, Z.F. Song, Z.A. Zhu, Hydrothermal fabrication of ZSM-5 zeolites: biocompatibility, drug delivery property, and bactericidal property, J Biomed Mater Res - Part B Appl Biomater. 102 (2014) 583–591, https://doi.org/10.1002/jbm.b.33037.

[8] N. Miriyala, D. Ouyang, Y. Perrie, D. Lowry, D.J. Kirby, Activated carbon as a carrier for amorphous drug delivery: effect of drug characteristics and carrier wettability, Eur. J. Pharm. Biopharm. 115 (2017) 197–205, https://doi.org/10.1016/j.ejpb.2017.03.002.

[9] B.S. Wong, S.L. Yoong, A. Jagusiak, T. Panczyk, H.K. Ho, W.H. Ang, G. Pastorin, Carbon nanotubes for delivery of small molecule drugs, Adv. Drug Deliv. Rev. 65 (2013) 1964–2015, https://doi.org/10.1016/j.addr.2013.08.005.

[10] R.C. Huxford, J. Della Rocca, W. Lin, Metal-organic frameworks as potential drug carriers, Curr. Opin. Chem. Biol. 14 (2010) 262–268, https://doi.org/10.1016/j.cbpa.2009.12.012.

[11] F.R.S. Lucena, L.C.C. de Araújo, M. do D. Rodrigues, T.G. da Silva, V.R.A. Pereira, G.C.G. Militão, D.A.F. Fontes, P.J. Rolim-Neto, F.F. da Silva, S.C. Nascimento, Induction of cancer cell death by apoptosis and slow release of 5-fluoracil from metal-organic frameworks Cu-BTC, Biomed Pharmacother 67 (2013) 707–713, https://doi.org/10.1016/j.biopha.2013.06.003.

[12] M.H. Teplensky, M. Fantham, P. Li, T.C. Wang, J.P. Mehta, L.J. Young, P.Z. Moghadam, J.T. Hupp, O.K. Farha, C.F. Kaminski, D. Fairen-Jimenez, Temperature treatment of highly porous zirconium-containing metal-organic frameworks extends drug delivery release, J. Am. Chem. Soc. 139 (2017) 7522–7532, https://doi.org/10.1021/jacs.7b01451.

[13] X. Zhao, S. Liu, C. Hu, Y. Liu, M. Pang, J. Lin, Controllable synthesis of monodispersed NU-1000 drug carrier for chemotherapy, ACS Appl Bio Mater. 2 (2019) 4436–4441, https://doi.org/10.1021/acsabm.9b00621.

[14] H.L. Wang, H. Yeh, B.H. Li, C.H. Lin, T.C. Hsiao, D.H. Tsai, Zirconium-based metal-organic framework nanocarrier for the controlled release of ibuprofen, ACS Appl Nano Mater. 2 (2019) 3329–3334, https://doi.org/10.1021/acsanm.9b00834.

[15] K.A. Mocniak, I. Kubajewska, D.E.M. Spillane, G.R. Williams, R.E. Morris, Incorporation of cisplatin into the metal-organic frameworks UiO66-NH2 and UiO66-encapsulation vs. conjugation, RSC Adv. 5 (2015) 83648–83656, https://doi.org/10.1039/c5ra14011k.

[16] L. Latifi, S. Sohrabnezhad, Drug delivery by micro and meso metal-organic frameworks, Polyhedron. 180 (2020) 114321, https://doi.org/10.1016/j.poly.2019.114321.

[17] Q. Chen, Q.W. Chen, C. Zhuang, P.P. Tang, N. Lin, L.Q. Wei, Controlled release of drug molecules in metal–organic framework material HKUST-1, Inorg. Chem. Commun. 79 (2017) 78–81, https://doi.org/10.1016/j.inoche.2017.03.027.

[18] T.C. Wang, N.A. Vermeulen, I.S. Kim, A.B.F. Martinson, J. Fraser Stoddart, J.T. Hupp, O.K. Farha, Scalable synthesis and post-modification of a mesoporous metal-organic framework called NU-1000, Nat. Protoc. 11 (2016) 149–162, https://doi.org/10.1038/nprot.2016.001.

[19] T. Grant Glover, G.W. Peterson, B.J. Schindler, D. Britt, O. Yaghi, MOF-74 building unit has a direct impact on toxic gas adsorption, Chem. Eng. Sci. 66 (2011) 163–170, https://doi.org/10.1016/j.ces.2010.10.002.

[20] F. Luo, C. Yan, L. Dang, R. Krishna, W. Zhou, H. Wu, X. Dong, Y. Han, T.L. Hu, M. O'Keeffe, L. Wang, M. Luo, R.B. Lin, B. Chen, UTSA-74: a MOF-74 isomer with two accessible binding sites per metal center for highly selective gas separation, J. Am. Chem. Soc. 138 (2016) 5678–5684, https://doi.org/10.1021/jacs.6b02030.

[21] H. Mirzaei, M. Darroudi, Zinc oxide nanoparticles: biological synthesis and biomedical applications, Ceram. Int. 43 (2017) 907–914, https://doi.org/10.1016/j.ceramint.2016.10.051.

[22] S. Javanbakht, P. Nezhad-Mokhtari, A. Shaabani, N. Arsalani, M. Ghorbani, Incorporating Cu-based metal-organic framework/drug nanohybrids into gelatin microsphere for ibuprofen oral delivery, Mater Sci Eng C. 96 (2019) 302–309, https://doi.org/10.1016/j.msec.2018.11.028.

[23] P. Horcajada, C. Serre, G. Maurin, N.A. Ramsahye, F. Balas, M. Vallet-Regí, M. Sebban, F. Taulelle, G. Férey, Flexible porous metal-organic frameworks for a controlled drug delivery, J. Am. Chem. Soc. 130 (2008) 6774–6780, https://doi.org/10.1021/ja710973k.

[24] P. Horcajada, C. Serre, M. Vallet-Regí, M. Sebban, F. Taulelle, G. Férey, Metal-organic frameworks as efficient materials for drug delivery, Angew Chemie - Int Ed. 45 (2006) 5974–5978, https://doi.org/10.1002/anie.200601878.

[25] Q. Hu, J. Yu, M. Liu, A. Liu, Z. Dou, Y. Yang, A low cytotoxic cationic metal-organic framework carrier for controllable drug release, J. Med. Chem. 57 (2014) 5679–5685, https://doi.org/10.1021/jm5004107.

[26] Z. Han, L. Lu, L. Wang, Z. Yan, X. Wang, Development and validation of an HPLC method for simultaneous determination of ibuprofen and 17 related compounds, Chromatographia. 80 (2017) 1353–1360, https://doi.org/10.1007/s10337-017-3358-3.

[27] A.L. Doadrio, E.M.B. Sousa, J.C. Doadrio, J. Pérez Pariente, I. Izquierdo-Barba, M. Vallet-Regí, Mesoporous SBA-15 HPLC evaluation for controlled gentamicin drug delivery, J. Control. Release 97 (2004) 125–132, https://doi.org/10.1016/j.jconrel.2004.03.005.

[28] K.S.W. Sing, R.T. Williams, Review Physisorption Hysteresis Loops and the Characterization of Nanoporous Materials, (2004), pp. 773–782, https://doi.org/10.1260/0263617053499032.

[29] I. Ahmed, S.H. Jhung, Applications of metal-organic frameworks in adsorption/separation processes via hydrogen bonding interactions, Chem. Eng. J. 310 (2017) 197–215, https://doi.org/10.1016/j.cej.2016.10.115.

[30] M. Carlo, C. Bernini, D. Fairen-jimenez, M. Pasinetti, A.J. Ramirez, Screening of biocompatible metal-organic frameworks as potential drug carriers using Monte Carlo Simulations, J Mater Chem B 2 (2014) 766–774, https://doi.org/10.1039/c3tb21328e.

[31] K. Tan, S. Zuluaga, Q. Gong, Y. Gao, N. Nijem, J. Li, T. Thonhauser, Y.J. Chabal, Competitive coadsorption of CO2 with H2O, NH3, SO2, NO, NO2, N2, O2, and CH4 in M-MOF-74 (M = Mg, Co, Ni): the role of hydrogen bonding, Chem. Mater. 74 (2015) 2203–2217, https://doi.org/10.1021/acs.chemmater.5b00315.

[32] S. Rojas, I. Colinet, D. Cunha, T. Hidalgo, F. Salles, C. Serre, N. Guillou, P. Horcajada, Toward understanding drug incorporation and delivery from biocompatible metal-organic frameworks in view of cutaneous administration, ACS Omega. 3 (2018) 2994–3003, https://doi.org/10.1021/acsomega.8b00185.

[33] X.G. Wang, Z.Y. Dong, H. Cheng, S.S. Wan, W.H. Chen, M.Z. Zou, J.W. Huo, H.X. Deng, X.Z. Zhang, A multifunctional metal-organic framework based tumor targeting drug delivery system for cancer therapy, Nanoscale. 7 (2015) 16061–16070, https://doi.org/10.1039/c5nr04045k.

[34] H. Li, N. Lv, X. Li, B. Liu, J. Feng, X. Ren, T. Guo, D. Chen, J. Fraser Stoddart, R. Gref, J. Zhang, Composite CD-MOF nanocrystals-containing microspheres for sustained drug delivery, Nanoscale. 9 (2017) 7454–7463, https://doi.org/10.1039/c6nr07593b.

[35] I.R.T. Haas, W. Windsor, F. Search, T. Pharmacological, 11 patent number: (9) sefensmestions and clinical trial of liquid analgesics, International Jour (1989) 4,861,797.